

# Impact of Thermal Conditions on Predicted Formability of TRIP Steels



Daniel S. Connolly, Christopher P. Kohar, Raja K. Mishra, and Kaan Inal

**Abstract** To improve vehicle fuel economy and improve safety, automakers have focussed on substituting low-carbon steel for advanced high-strength steel (AHSS) alloys. A common grade of AHSS is the transformation-induced plasticity (TRIP) steels, which undergo a phase transformation from austenite to martensitic that enhances the ductility and strength. This work employs a phenomenological constitutive model for TRIP 800 steel to study the thermomechanical behaviour over large strains. This formulation is implemented into the recently developed fully coupled thermomechanical Marciniak–Kuczynski (MK) framework by Connolly et al. (2018). These are employed to analyze formability of a TRIP 800 alloy under a range of thermal conditions expected in realistic stamping operations. This work demonstrates that control of the initial blank temperature, die temperature, and die conduction coefficient can produce improvements in uniaxial and plane strain formability of up to 44% and 41% relative to room temperature formability. In contrast, the presented study shows that poor control of these parameters can reduce uniaxial and plane strain formability by up to 35% and 41%. Additionally, the conditions for optimal formability are shown to be strain path dependent, suggesting that tightly coupling component, process, and die design could improve final component designs.

**Keywords** TRIP steel · M–K-based forming limit diagrams · Thermomechanical modelling

---

D. S. Connolly (✉) · C. P. Kohar · K. Inal  
Department of Mechanical and Mechatronics Engineering, University of Waterloo, Waterloo N2L 3G1, Canada  
e-mail: [dconnol@uwaterloo.ca](mailto:dconnol@uwaterloo.ca)

R. K. Mishra  
General Motors Research & Development Center, Warren, MI 48090, USA

## Introduction

Structural lightweighting through the novel design technology development [1] and advanced material substitution [2–4] has been a focus for automakers to address vehicle fuel economy regulations [5]. For formability components, particular focus has been directed to the development of novel advanced high-strength steel (AHSS) alloys due to their high strength and ductility. These desirable characteristics result from advanced chemical compositions and heat treatment processes allowing fine control of phase properties with these multiphase alloys. In addition, AHSS alloys commonly exhibit the transformation-induced plasticity (TRIP) effect, wherein metastable retained austenite ( $\gamma$ ) transforms into martensite ( $\alpha'$ ). This effect depends on temperature [6], stress state [7], and strain rate [8], and can induce tension–compression asymmetry in yield behaviour [9]. This results in substantial increase in material hardening, improving ductility, strength, and fracture resistance [10]. The most industrially applicable steels exhibiting this behaviour are TRIP steels, wherein the retained austenite (RA) and martensite exist within a matrix of ferrite ( $\alpha$ ) and bainite ( $\beta$ ) [11].

To enable rapid and cost-effective design iteration, vehicles are designed primarily in a virtual environment, with experiments used as calibration and validation. Component design is then limited by a combination of formability, weight, energy absorption, and strength (i.e., anti-penetration). One formability measure is the forming limit diagram (FLD) [12, 13], which is defined as a set of limit strains below which a sheet metal deformed under a constant strain path is unlikely to fail through localized necking. A common approach for numerically predicting an FLD is the Marciniak–Kuczynski (MK) analysis [14], wherein analytical equations are used to model the evolution of a diffuse neck.

Connolly et al. [15] recently extended MK analysis to include a fully coupled thermal model. This was coupled with an advanced constitutive model to analyze the effects of transformation deformation kinematics and thermal conditions on the formability of a TRIP 800 steel alloy. Their results showed that control of the thermal boundary conditions and initial blank temperature could be used to improve formability by up to 35% in uniaxial tension and 25% in plane strain tension. This work builds upon these results by analyzing formability under a realistic forming process, controlling initial blank temperature, stamping die temperature, and the stamping die to blank conduction coefficient to suggest specific avenues of exploration for improving formability in existing TRIP steel alloys.

## Model Formulation

### Constitutive Modeling

This work employs the phenomenological model previously used in Kohar et al. [16] and Connolly et al. [15]. This model is summarized below with full details in the aforementioned paper.

### Strain-Rate Decomposition

The total strain rate,  $\dot{\epsilon}_{ij}$ , is decomposed into elastic ( $\dot{\epsilon}_{ij}^{elast}$ ), inelastic ( $\dot{\epsilon}_{ij}^p$ ), and thermal ( $\dot{\epsilon}_{ij}^{therm}$ ) terms:

$$\dot{\epsilon}_{ij} = \dot{\epsilon}_{ij}^{elast} + \dot{\epsilon}_{ij}^p + \dot{\epsilon}_{ij}^{therm} \quad (1)$$

The thermal strain rate can be modelled using isotropic thermal expansion, given by

$$\dot{\epsilon}_{ij}^{therm} = \alpha_L \delta_{ij} \dot{T} \quad (2)$$

where  $\alpha_L$  is the linear thermal expansion coefficient,  $\delta_{ij}$  is the Kronecker delta, and  $\dot{T}$  is the temperature rate. The inelastic deformation is further decomposed into plastic slip strain ( $\dot{\epsilon}_{ij}^{pslip}$ ) and both a dilational ( $\dot{\epsilon}_{ij}^{pdilat}$ ) and shape change ( $\dot{\epsilon}_{ij}^{pshape}$ ) component of transformation strain:

$$\dot{\epsilon}_{ij}^p = \dot{\epsilon}_{ij}^{pslip} + \dot{\epsilon}_{ij}^{pdilat} + \dot{\epsilon}_{ij}^{pshape} \quad (3)$$

The plastic slip strain is given by the associative flow rule

$$\dot{\epsilon}_{ij}^{pslip} = \dot{\bar{\epsilon}}^{pslip} \frac{\partial \Phi}{\partial \sigma_{ij}} \quad (4)$$

where  $\dot{\bar{\epsilon}}^{pslip}$  is the effective plastic slip rate and  $\Phi$  is the yield function. The dilational and shape change transformation strains are given by

$$\dot{\epsilon}_{ij}^{pdilat} = \frac{1}{3} \Delta V \dot{f}_{\alpha'} \delta_{ij} \quad (5)$$

$$\dot{\epsilon}_{ij}^{pshape} = \left[ R_0 + R_1 \left( \frac{\tilde{\sigma}_{eff}}{\sigma_{0,\gamma}} \right) \right] \dot{f}_{\alpha'} \frac{\partial \Phi}{\partial \sigma_{ij}} \quad (6)$$

where  $\Delta V = 0.02$  is the austenite to martensite volume change,  $R_0 = 0.02$  and  $R_1 = 0.02$  are fitted parameters,  $\tilde{\sigma}_{eff}$  is the effective flow stress,  $\sigma_{0,\gamma}$  is the austenite initial yield stress, and  $\dot{f}_{\alpha'}$  is the rate of transformation of martensite.

### Kinetics of Transformation

Martensite transformation rate is assumed to occur as a result of the formation of new martensitic units at potent nucleation sites at shear band intersections [6, 17]. The transformation rate is given by

$$\dot{f}_{\alpha'} = f_{\gamma} [p \dot{f}_{sb}^i + f_{sb}^i \dot{p} \theta(\dot{p})] \quad (7)$$

where  $f_{\gamma}$  is the austenite volume fraction,  $p$  is the probability of a shear band intersection site transforming,  $f_{sb}^i$  is the volume fraction of shear band intersection sites, and  $\theta(\star)$  is a Heaviside function. The shear band intersection volume fraction, shear band volume fraction ( $f_{sb}$ ), and effective slip rate in the austenite ( $\dot{\bar{\epsilon}}_{\gamma}^{pslip}$ ) are related using

$$f_{sb}^i = \eta (f_{sb})^{n_s} \quad (8)$$

$$\dot{f}_{sb} = a_m (1 - f_{sb}) \dot{\bar{\epsilon}}_{\gamma}^{pslip} \quad (9)$$

where  $\eta$  and  $n_s$  are calibration constants and  $a_m$  is given by

$$a_m = (a_{m,1} + a_{m,2}T + a_{m,3}T^2 - a_{m,4}\Sigma) \left( 1 - a_{m,5} \left( \frac{\dot{\bar{\epsilon}}}{\dot{\bar{\epsilon}}_0} \right)^{a_{m,6}} \right) \quad (10)$$

$$\Sigma = \frac{\text{tr}(\sigma)}{3\tilde{\sigma}} \quad (11)$$

where  $a_{m,1}$ - $a_{m,6}$  are calibration parameters,  $T$  is temperature,  $\Sigma$  is stress triaxiality,  $\dot{\bar{\epsilon}}$  is an effective strain rate,  $\dot{\bar{\epsilon}}_0$  is a normalization factor, and  $\tilde{\sigma}$  is the von Mises equivalent stress. The probability of transformation is given by

$$p = \frac{1}{\sqrt{2\pi}\sigma_s} \int_{-\infty}^g \exp\left(-\frac{(g' - g_0)^2}{2\sigma_s^2}\right) dg' \quad (12)$$

$$g = -T + g_1 \Sigma \quad (13)$$

where  $g_0$  and  $\sigma_s$  are the mean and standard deviation of the distribution of critical driving forces required to cause transformation at a shear band intersection site,  $g$  is the transformation driving force, and  $g_1$  is the dependence of the driving force triaxiality.

### Effective Flow Stress

It is assumed that the average effective flow stress ( $\bar{\sigma}_{ave}$ ) is given by a rule of mixtures such that

$$\bar{\sigma}_{ave} = f_\gamma \bar{\sigma}_\gamma + f_\beta \bar{\sigma}_\beta + f_\alpha \bar{\sigma}_\alpha + f_{\alpha'} \bar{\sigma}_{\alpha'} \quad (14)$$

where  $f_i$  and  $\bar{\sigma}_i$  are the volume fraction and effective stress of each phase as denoted by  $= \{\gamma, \beta, \alpha, \alpha'\}$ . The effective stress of each phase  $i$  is given using a Holloman hardening law:

$$\bar{\sigma}_i = K_i (\varepsilon_{0,i} + \bar{\varepsilon}^{pslip})^{n_i} \quad (15)$$

$$\varepsilon_{0,i} = \left( \frac{E_i}{K_i} \right)^{\frac{1}{n_i-1}} \quad (16)$$

where  $K_i$  and  $n_i$  are calibrated constants,  $\varepsilon_{0,i}$  is the yield strain, and  $E_i$  is Young's modulus. The Johnson–Cook [18] model is used to incorporate temperature sensitivity and the Cowper–Symonds [19] model is used to incorporate strain-rate sensitivity, such that the total flow stress,  $\bar{\sigma}$ , is given by

$$\bar{\sigma} = \bar{\sigma}_{ave} \left( 1 + \left( \frac{\dot{\varepsilon}}{C} \right)^{1/P} \right) \left( 1 - \left( \frac{T - T^*}{T_{melt} - T^*} \right)^m \right) \quad (17)$$

where  $C$  and  $P$  are Cowper–Symonds rate sensitivity parameters,  $\dot{\varepsilon}$  is the total effective strain rate,  $T^*$  is a reference temperature,  $T_{melt}$  is the material melting point, and  $m$  is a temperature sensitivity exponent.

### Evolving Anisotropic Yield Function

The yield surface is given by a modified Yld2000 function [20] with an evolving asymmetry term [9]:

$$\Phi = \phi(\sigma_{ij})^{\frac{1}{3}} + 3^{\frac{7}{6}} k \frac{J_3(\sigma_{ij})}{\phi(\sigma_{ij})^{1/6}} - \bar{\sigma}(\bar{\varepsilon}^{pslip}, T, \dot{\varepsilon})^2 = 0 \quad (18)$$

$$\dot{k} = C_k(1 - k)\dot{\bar{\epsilon}}^{pslip} \tag{19}$$

where  $\phi(\sigma_{ij})$  is the Yld2000 function,  $J_3$  is the third deviatoric stress tensor invariant,  $k$  is a parameter defining the evolving yield surface asymmetry, and  $C_k = 0.49$  [21] governs the asymmetry increase rate. A maximum limit is enforced for  $k$  such that yield surface convexity is maintained [15]. The overall constitutive equation for stress is given by a hypo-elastic formulation with a modified Jaumann co-rotational framework such that

$$\dot{\sigma}_{ij}^{\nabla J} = \mathcal{L}_{ijkl}^{el} \dot{\epsilon}_{kl}^{elast} \tag{20}$$

$$\dot{\sigma}_{ij} = \dot{\sigma}_{ij}^{\nabla J} + \sigma_{ik} W_{kj} - W_{ik} \sigma_{kj} + \sigma_{ij} \dot{\epsilon}_{kk} \tag{21}$$

where  $\mathcal{L}_{ijkl}^{el}$  is the isotropic elasticity tensor and  $W_{ij}$  is the antisymmetric component of the velocity gradient.

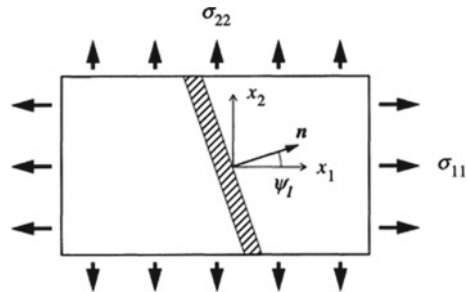
### Coupled Thermomechanical Marciniak–Kuczynski Analysis

This work uses the fully coupled thermal MK model outlined in Connolly et al. [15] which is utilized for this work. A brief description of the model is given here. Figure 1 [15] shows a schematic of an infinite sheet with axes  $x_1$  and  $x_2$  and an infinite band related by an initial angle  $\psi_I$  to the  $x_1$ -axis. A superscript  $B$  and no superscript are used to denote in-band and out-of-band properties, respectively. The band ( $H^B(t)$ ) and sheet ( $H(t)$ ) thicknesses are initially related through an imperfection parameter ( $f$ ):

$$f = \frac{H^B(0)}{H(0)} \tag{22}$$

The MK formulation assumes plane stress sheet deformation such that

**Fig. 1** Sheet with initial band inclined at angle  $\psi_I$



$$\dot{\varepsilon}_{22} = P\dot{\varepsilon}_{11}, W_{12} = \dot{\varepsilon}_{12} = 0 \quad (23)$$

where  $P$  is a proportionality constant. The band angle ( $\psi$ ) is updated by

$$\tan \psi = \exp[(1 - P)\varepsilon_{11}]\tan \psi_I \quad (24)$$

The in-band and out-of-band velocity gradients are related by [22]

$$L_{\alpha\beta}^B = L_{\alpha\beta} + \dot{g}_\alpha n_\beta \quad \alpha, \beta = 1, 2 \quad (25)$$

Force equilibrium requires that in-band and out-of-band stresses are related by

$$n_\alpha \sigma_{\alpha\beta}^B H^B = n_\alpha \sigma_{\alpha\beta} H \quad (26)$$

The numerical results are updated by solving algebraic equations for  $\dot{g}_\alpha$  and  $D_{33}^B$  created by combing the constitutive law, force equilibrium, and boundary conditions. Necking localization failure occurs when the in-band thickness strain rate ( $D_{33}^B$ ) is tenfold larger than the out-of-band thickness strain rate ( $D_{33}$ ). Temperature evolution in band and out of band is considered independently and is described by

$$\rho C_p T = \frac{2[R_f(1 - s_f)(T_{ext} - T) + s_f h_c(T_\infty - T) + s_f \sigma_b \epsilon_r (T_\infty^4 - T_4)]}{H} + (\chi \bar{\sigma} \dot{\varepsilon}^{pslip} + Q_{tr} f_{\alpha'}) \quad (27)$$

where  $R_f$  is a conductive heat transfer constant,  $T_{ext}$  is conductive boundary temperature,  $s_f$  is the surface fraction exposed to air,  $h_c$  is a convective heat transfer coefficient,  $T_\infty$  is the air temperature,  $\sigma_b = 5.67 \times 10^{-8} W/m^2 K$  is the Stefan–Boltzmann constant,  $\epsilon_r$  is a coefficient of emissivity,  $\chi = 0.9$  is the plastic work fraction converted into heat, and  $Q_{tr}$  is the specific latent heat of austenite to martensite transformation.

## Material Characterization and Calibration

This work uses coefficients presented in Connolly et al. [15] as summarized here. Table 1 presents the elastic and plastic parameters for each phase and Table 2 presents the TRIP 800 steel thermal properties.

Table 3 lists the yield function coefficients as calibrated to experimental Lankford coefficients and normalized yield stress variation with  $k = 0$  and with the coefficient ranges restricted to  $\alpha_i \in [0.8, 1.2]$ . The maximum asymmetry coefficient with these parameters was determined to be  $k_{lim} = 0.762$ .

**Table 1** Elasticity and hardening parameters for TRIP800 [15]

	$f_i$ [%]	$E_i$ [GPa]	$\nu_i$	$K_i$ [MPa]	$n_i$	$\epsilon_0 (\times 10^{-3})$
Austenite, $\gamma$	16.5	190	0.30	1300	0.114	3.602
Bainite, $\beta$	13.5	210	0.30	2930	0.201	4.776
Ferrite, $F$	70.0	210	0.30	720	0.135	1.416
Martensite, $\alpha'$	0.0	210	0.30	3470	0.126	9.133

**Table 2** Thermal properties of TRIP 800 steel

	TRIP 800
Density, $\rho$ [ $gm^{-3}$ ]	7800
Specific heat capacity, $C_p$ [ $Jkg^{-1}K^{-1}$ ]	519
Thermal expansion, $\alpha_L$ [ $K^{-1}$ ]	$12 \times 10^{-6}$
Thermal resistance, $R_f''$ [ $Wm^{-2}K^{-1}$ ]	22
Coefficient of convection, $h''$ [ $Wm^{-2}K^{-1}$ ]	15
Emissivity coefficient, $\epsilon''$	0.80
Fraction of exposed surface to air, $s_f$	0.50

**Table 3** Yld2000 yield function parameters for TRIP 800

$\alpha_1$	$\alpha_2$	$\alpha_3$	$\alpha_4$	$\alpha_5$	$\alpha_6$	$\alpha_7$	$\alpha_8$	a
0.9719	0.9882	1.1051	0.9634	0.9882	0.8918	1.0214	0.8980	6.00

Tables 4 and 5 present the calibrated parameters for martensite transformation, Johnson–Cook thermal sensitivity, and Cowper–Symonds strain rate sensitivity. These were determined via simultaneous calibration to flow stress for several temperatures and strain rates, martensite evolution for several strain rates and strain paths, and temperature rise under uniaxial tension at an elevated strain rate.

**Table 4** Flow stress strain rate and temperature sensitivity parameters for TRIP 800

$C$ [ $s^{-1}$ ]	$P$	$\dot{\epsilon}_0$ [ $s^{-1}$ ]	$m$	$T^*$ [K]	$T_{meli}$ [K]	$\chi$	$Q_{tr}$ [ $Wm^{-3}$ ]
$9.938 \times 10^4$	5.2554	$1.0 \times 10^{-4}$	1.274	293	1643	0.90	$4.981 \times 10^9$

**Table 5** Martensite generation parameters for TRIP 800

$a_{m,1}$	$a_{m,2}$	$a_{m,3}$	$a_{m,4}$	$a_{m,5}$	$a_{m,6}$	$\sigma_g$	$g_0$	$g_1$	$\eta$	$n_s$
1.698	$5.865 \times 10^{-2}$	$-1.137 \times 10^{-4}$	-4.320	0.09864	0.153	335.12	0.0071	76.8	9.626	4.058



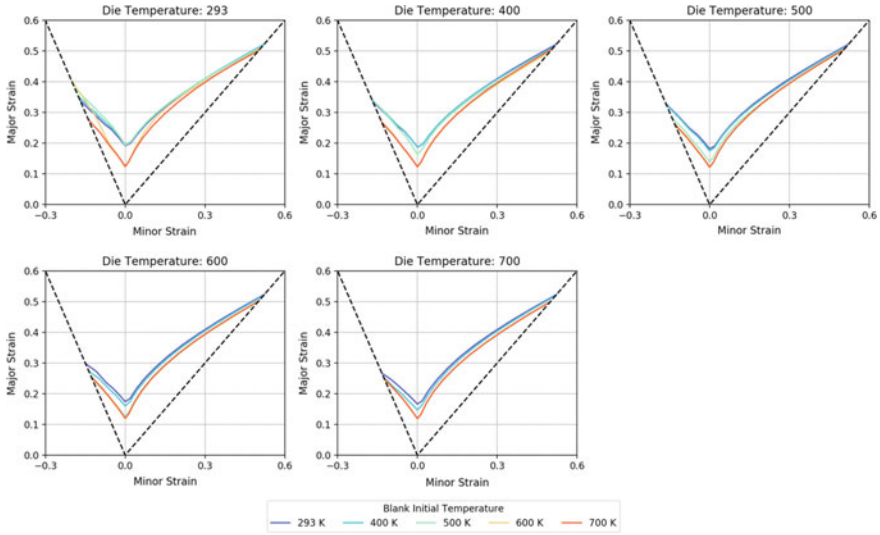
## Results and Discussion

The purpose of this work is to study the influence of thermal processing parameters on formability of TRIP 800 steel during a forming operation. In forming processes where the blank is typically constrained in a fixture that is not exposed to the surroundings, conduction to the forming dies is the main heat transfer mechanism. In practice, the conduction coefficient can be modified through selective lubricants and die design. It should be stressed that the conduction coefficient used here is meant to represent the overall heat transfer between the blank surface and a thermal boundary (e.g., coolant) and will therefore be much lower than the conduction between the blank and the die surface.

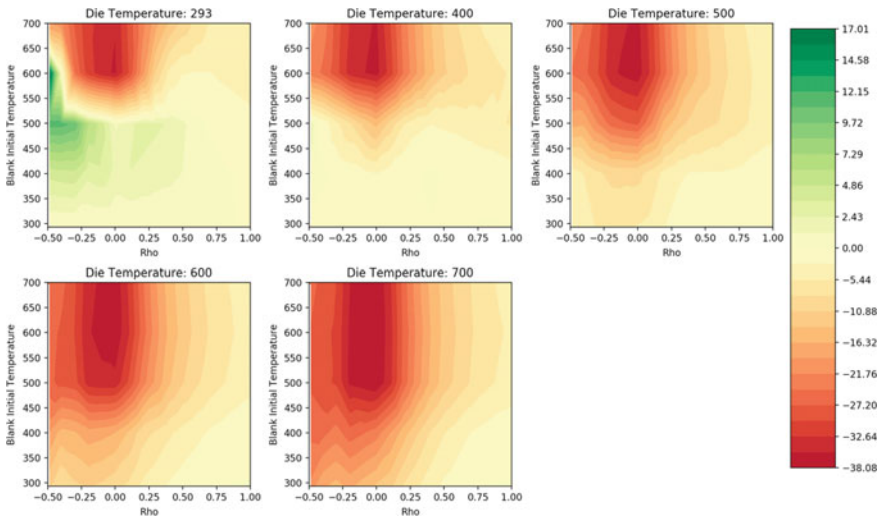
In this study, the thermal conductivity coefficient is varied to explore the effect on formability through modification of the martensite generation rate in the sheet. It is assumed that the entire surface of the sheet is in contact with the dies, such that convective and radiative heat transfer can be neglected ( $s_f = 0$ ). The conduction coefficients used are  $R_f = \{10, 20, 40, 80\} \text{ Wm}^{-2}\text{K}^{-1}$ . The initial temperature of the blank,  $T(0)$ , and external thermal BCs varied between  $400\text{K}$  and  $700\text{K}$  with  $\Delta T(0) = \Delta T_{ext} = 100\text{K}$  and compared to formability with a blank initially at room temperature ( $T(0) = 293\text{K}$ ) and with room temperature dies ( $T_{ext} = 293\text{K}$ ). The independent variables of this study are the initial blank temperature ( $T(0)$ ), the external boundary temperature ( $T_{ext}$ ), and the conduction coefficient ( $R_f$ ). Each formability study was conducted with a macroscopic strain rate,  $D_{11} = 1.0 \times 10^{-3}\text{s}^{-1}$ , an imperfection parameter,  $f = 0.996$  [23], proportionality constant of  $-0.5 \leq P \leq 1.0$  with  $\Delta P = 0.1$ , and initial band angle of  $0^\circ \leq \psi_I \leq 40^\circ$  with  $\Delta\psi_I = 5^\circ$ .

Figure 2 presents the FLD for an effective conduction coefficient of  $R_f = 10\text{Wm}^{-2}\text{K}^{-1}$  for different initial temperature conditions. The percentage improvement in formability for a given initial blank temperature, thermal boundary condition, and strain path for the same strain path for an initial blank temperature and boundary temperature of  $293\text{K}$  and conduction coefficient of  $10\text{Wm}^{-2}$  is presented in Fig. 3. Raising the initial blank temperature for a constant die temperature results in two possible effects depending on the die temperature. For room temperature external BCs, increasing the initial blank temperature primarily had the effect of delaying martensite generation, while also resulting in minor reductions in the final volume fraction of martensite generated. This yielded a net improvement in formability, up until the critical temperature discussed in Connolly et al. [15], where the blank does not chill sufficiently for transformation to initiate. Throughout this work, this point will be referred to as the critical blank temperature. However, at elevated die temperatures, raising the initial blank temperature resulted in a major reduction in the final volume fraction of martensite. This yielded a net reduction in formability.

Figures 4, 5, 6 present the percentage improvement in formability for a given initial blank temperature, die temperature, and strain path with  $R_f = \{20, 40, 80\} \text{ Wm}^{-2}\text{K}^{-1}$  relative to the formability with boundary and die temperatures of  $293\text{K}$



**Fig. 2** Predicted forming limit diagrams for an effective conduction coefficient of  $10 \text{ W m}^{-2} \text{ K}^{-1}$  for a variety of boundary temperatures and initial blank temperatures



**Fig. 3** Predicted percentage improvement in forming limit strain comparing an effective conduction coefficient of  $10 \text{ W m}^{-2} \text{ K}^{-1}$  for a variety of boundary temperatures and initial blank temperatures to an effective conduction coefficient of  $10 \text{ W m}^{-2} \text{ K}^{-1}$  with boundary temperature 293 K and initial blank temperature 293 K

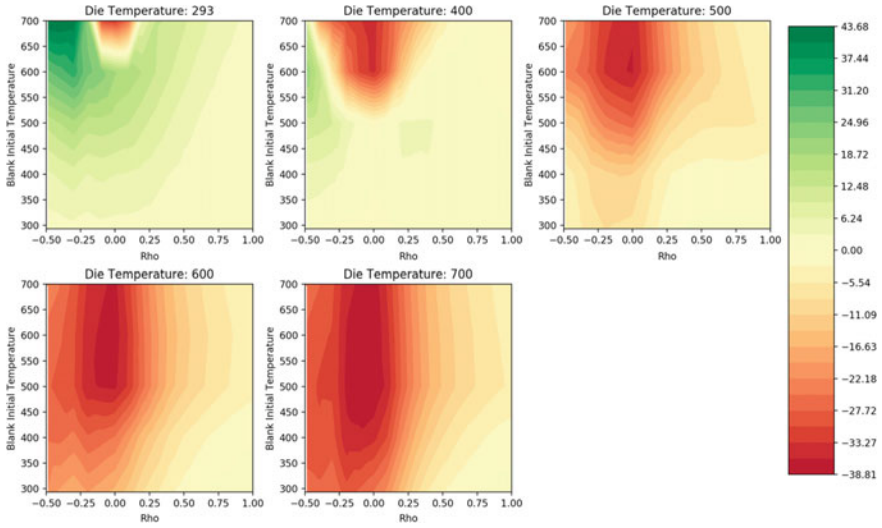


**Fig. 4** Predicted percentage improvement in forming limit strain comparing an effective conduction coefficient of  $20 \text{ W m}^{-2} \text{ K}^{-1}$  for a variety of boundary temperatures and initial blank temperatures to an effective conduction coefficient of  $10 \text{ W m}^{-2} \text{ K}^{-1}$  with boundary temperature 293 K and initial blank temperature 293 K

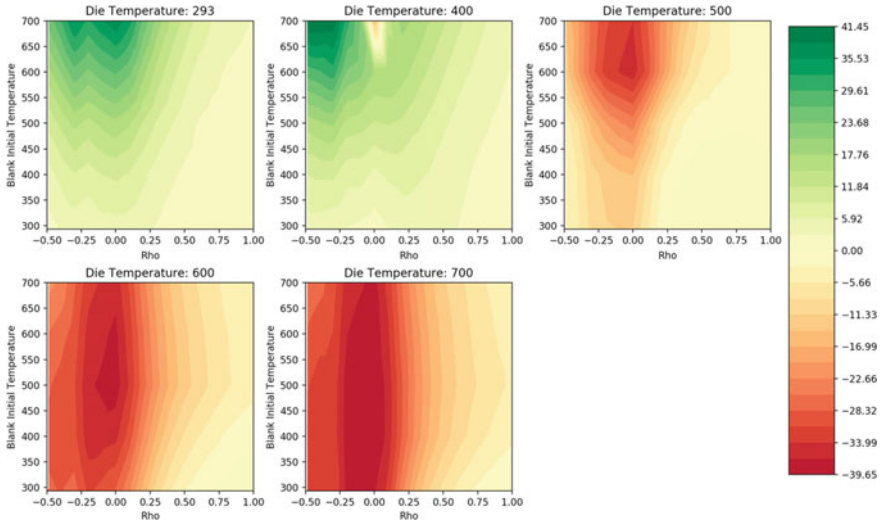


**Fig. 5** Predicted percentage improvement in forming limit strain comparing an effective conduction coefficient of  $40 \text{ W m}^{-2} \text{ K}^{-1}$  for a variety of boundary temperatures and initial blank temperatures to an effective conduction coefficient of  $10 \text{ W m}^{-2} \text{ K}^{-1}$  with boundary temperature 293 K and initial blank temperature 293 K

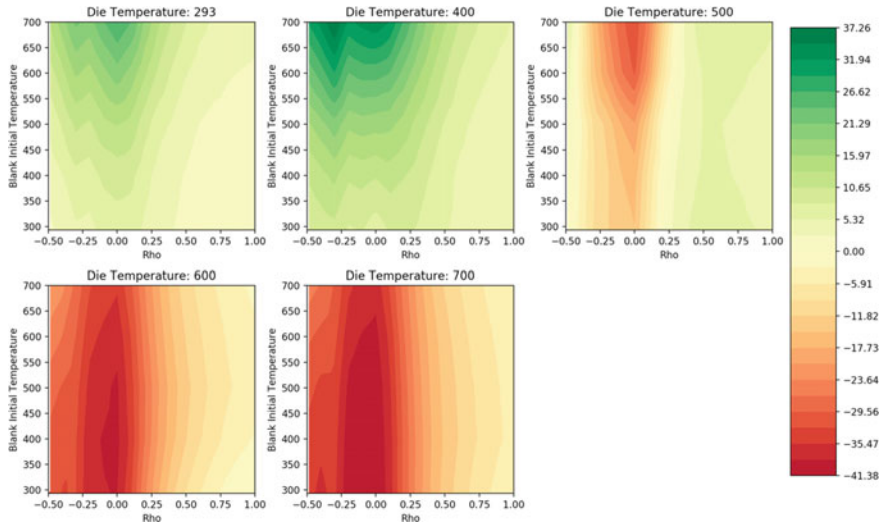


**Fig. 6** Predicted percentage improvement in forming limit strain comparing an effective conduction coefficient of  $80 \text{ W m}^{-2} \text{ K}^{-1}$  for a variety of boundary temperatures and initial blank temperatures to an effective conduction coefficient of  $10 \text{ W m}^{-2} \text{ K}^{-1}$  with boundary temperature 293 K and initial blank temperature 293 K

and a conduction coefficient of  $10 \text{ W m}^{-2}$ . The effect of increased blank temperature with room temperature dies and elevated conduction coefficients is similar to the low conduction case: increasing blank temperature leads to an increase in formability until reaching the critical blank temperature. However, unlike the low condition case, simultaneously increasing blank and die temperatures can result in a net improvement in formability for moderate die temperatures (400 K and 500 K). This is because the elevated die conduction coefficient allows cooling to occur faster, allowing martensite formation to begin earlier and continue longer. Despite an increase in the conduction coefficient, the high die temperature cases (600 K and 700 K) did not result in an increase in formability. This is because transformation is almost completely suppressed at these temperatures, where little transformation occurs despite the blank reaching the die temperature.

It is important to understand the overall sensitivity of formability to initial blank temperature, die temperature, and conduction coefficient to optimize the thermal parameters. Considering only cases with room temperature or moderate die temperature and a blank temperature beneath the critical blank temperature, formability is improved with decreasing die coefficient, increasing initial blank temperature, and increasing die temperature. Conversely, the value of the critical blank temperature itself increases with increasing die coefficient and decreasing die temperature. In a forming process, the critical blank temperature limits the maximum formability of a process. Improving formability requires finding the correct process parameters to simultaneously increase the critical blank temperature while improving formability

below the critical blank temperature. Since the critical blank temperature is dependent on the strain path of deformation, the optimal choice of process parameters will likely be dependent on the expected strain paths of the specific component being formed.

In this study, the maximum uniaxial tension formability was predicted to occur with a boundary temperature of 293 K, a conduction coefficient of  $20 \text{ W m}^{-2}$ , and an initial blank temperature of 700 K. These conditions resulted in a uniaxial tension formability improvement from 0.33 to 0.48 strain (+44%), but also caused a reduction in plane strain formability from 0.19 to 0.14 (−27%). The maximum plane strain formability occurred with a boundary temperature of 293 K, a conduction coefficient of  $40 \text{ W m}^{-2}$ , and an initial blank temperature of 700 K. With these conditions, plane strain formability improved from 0.19 to 0.26 (41%) and uniaxial formability improved from 0.33 to 0.41 (26%). As in Connolly et al. [15], there are only minor effects on the equibiaxial side because the yield surface changes are decoupled from the martensite generation, and the martensite generation is saturated and therefore has minimal effect on hardening at the localization strain. In this study, the blank temperature, die temperature, and conduction coefficient. In an unbounded optimization, larger improvements could likely be obtained. Additionally, it is crucial to recognize that poor control of thermal process parameters may also result in significant reductions in formability. The worst case obtained in the study had an initial blank temperature of 293 K, die temperature of 700 K, and a conduction coefficient of  $80 \text{ W m}^{-2}$ . In this case, uniaxial formability reduced from 0.33 to 0.21 (−35%), plane strain formability reduced from 0.19 to 0.11 (−41%), and equibiaxial formability is unchanged.

## Conclusion

In this paper, the formability behaviour of a TRIP 800 steel subject to realistic thermal conditions for forming processes was analyzed. It employed the constitutive model and fully coupled thermomechanical MK analysis presented in Connolly et al. [15]. This study varied the effective conduction coefficient, blank temperature, and die temperature to obtain the following specific conclusions:

- Hot forming of TRIP steels using in-die cooling can result in improvements in predicted formability of up to 44% under uniaxial tension and 41% under plane strain tension were observed.
- Excessive blank and die heating can result in reductions in predicted formability of up to 35% under uniaxial tension and 41% under plane strain tension were observed
- Optimal thermal process parameters depend on strain path, suggesting that the ideal formability curve is tightly coupled to die and component design

**Acknowledgements** This work was supported by the Natural Sciences and Engineering Research Council-Automotive Partnership Collaboration (NSERC-APC) under grant no. APCJ 441668-12, Natural Sciences and Engineering Research Council-Industrial Research Chair (NSERC-IRC) under grant no. IRCPJ-503185-2016, and General Motors of Canada. The first author (D.S.C.) would like to acknowledge the Natural Sciences and Engineering Research Council-Undergraduate Student Research Award for financial support that was provided. The second author (C.P.K.) would like to acknowledge the Ontario Graduate Scholarship for their financial support that was provided.

## References

1. Kohar CP, Zhumagulov A, Brahme A, Worswick MJ, Mishra RK, Inal K (2016) Development of high crush efficient, extrudable aluminium front rails for vehicle lightweighting. *Int J Impact Eng* 95:17–34
2. Kohar CP, Bassani JL, Brahme A, Muhammad W, Mishra RK, Inal K (2019) A new multi-scale framework to incorporate microstructure evolution in phenomenological plasticity: theory, explicit finite element formulation, implementation and validation. *Int J Plast* 117:122–156
3. Zhang P, Kohar CP, Brahme AP, Choi S-H, Mishra RK, Inal K (2019) A crystal plasticity formulation for simulating the formability of a transformation induced plasticity steel. *J Mater Process Technol*:116493
4. Connolly D, Kohar C, Muhammad W, Hector LG, Mishra RK, Inal K (2020) A coupled thermomechanical crystal plasticity model applied to quenched and partitioned steel. *Int J Plast*. Under Review
5. U.S.E.P.A. (2016) Draft technical assessment report: midterm evaluation of light-duty vehicle greenhouse gas emission standards and corporate average fuel economy standards for model years 2022–2025. U.S. Environmental Protection Agency, Washington, D.C.
6. Olson GB, Cohen M (1975) Kinetics of strain-induced martensitic nucleation. *MTA* 6(4):791
7. Iwamoto T, Tsuta T, Tomita Y (1998) Investigation on deformation mode dependence of strain-induced martensitic transformation in trip steels and modelling of transformation kinetics. *Int J Mech Sci* 40(2):173–182
8. Tomita Y, Iwamoto T (1995) Constitutive modeling of trip steel and its application to the improvement of mechanical properties. *Int J Mech Sci* 37(12):1295–1305
9. Miller MP, McDowell DL (1996) Modeling large strain multiaxial effects in FCC polycrystals. *Int J Plast* 12(7):875–902
10. Wu R, Li W, Zhou S, Zhong Y, Wang L, Jin X (2014) Effect of retained austenite on the fracture toughness of quenching and partitioning (Q&P)-treated sheet steels. *Metall Mater Trans A* 45(4):1892–1902
11. Bhandarkar D, Zackay VF, Parker ER (1972) Stability and mechanical properties of some metastable austenitic steels. *MT* 3(10):2619–2631
12. Keeler S, Backofen W (1963) Plastic instability and fracture in sheets stretched over rigid punches. *ASM Trans Q* 56(1):25–48
13. Goodwin GM (1968) Application of strain analysis to sheet metal forming problems in the press shop. *SAE Papers*
14. Marciniak Z, Kuczyński K (1967) Limit strains in the processes of stretch-forming sheet metal. *Int J Mech Sci* 9(9):609–620
15. Connolly DS, Kohar CP, Mishra RK, Inal K (2018) A new coupled thermomechanical framework for modeling formability in transformation induced plasticity steels. *Int J Plast* 103:39–66
16. Kohar CP, Cherkaoui M, El Kadiri H, Inal K (2016) Numerical modeling of TRIP steel in axial crashworthiness. *Int J Plast* 84:224–254

17. Stringfellow RG, Parks DM, Olson GB (1992) A constitutive model for transformation plasticity accompanying strain-induced martensitic transformations in metastable austenitic steels. *Acta Metall Mater* 40(7):1703–1716
18. Johnson GR, Cook H (1983) A constitutive model and data for metals subjected to large strains, high strain rates and high temperatures. In: *Proceedings of the 7th international symposium on ballistics*, The Hague, Netherlands, pp 541–547
19. Cowper G, Symonds P (1957) *Strain-hardening and strain-rate effects in the impact loading of cantilever beams*. Brown University Division of Applied Mathematics, Providence, Rhode Island, USA
20. Barlat F, Brem JC, Yoon JW, Chung K, Dick RE, Lege DJ et al (2003) Plane stress yield function for aluminum alloy sheets—part 1: theory. *Int J Plast* 19(9):1297–1319
21. Dan WJ, Zhang WG, Li SH, Lin ZQ (2007) Finite element simulation on strain-induced martensitic transformation effects in TRIP steel sheet forming. *Comput Mater Sci* 39(3):593–599
22. Hutchinson JW, Neale KW (1978) Sheet necking. II. Time independent behaviour. III. Strain-rate effects. In: Koistinen D, Wang N-M (eds) *Mechanics of sheet metal forming*. Plenum Publishing Corporation, New York, pp 269–285
23. Barlat F, Richmond O (2003) Modelling macroscopic imperfections for the prediction of flow localization and fracture. *Fatigue Fract Eng Mater Struct* 26(4):311–321